Asian Journal of Chemistry; Vol. 37, No. 6 (2025), 1307-1314

ASIAN JOURNAL OF CHEMISTRY

https://doi.org/10.14233/ajchem.2025.33697

Layered Zn doped WO_3 Nanoplates Fabricated *via* Hydrothermal Method for Efficient Photocatalytic Degradation of Congo Red Dye

SUNIL G. SHELAR[1,2], SANDIP P. PATIL[3], VILAS K. MAHAJAN[1], P.K. LABHANE[4], B.S. BHADANE[1], A.D. MUDAWADKAR[1] and GUNVANT H. SONAWANE[1,*]

[1]Department of Chemistry, K.V.P.S. Kisan Arts, Commerce and Science College, Parola-425111, India
[2]Department of Chemistry, S.R.N.D. Arts, Commerce and Science College, Bhadgaon-424105, India
[3]Nano-Chemistry Research Laboratory, N.T.V.S.'s G.T. Patil Arts, Commerce and Science College, Nandurbar-425412, India
[4]Department of Chemistry, MGSM's Dadasaheb Dr. Suresh G. Patil College, Chopda-425107, India

*Corresponding author: E-mail: drgunvantsonawane@gmail.com

Received: 8 March 2025; *Accepted*: 20 April 2025; *Published online*: 27 May 2025; AJC-22002

Orthorhombic Zn doped WO_3 nanoplates (1, 2 and 5 wt.%) were fabricated by a simple and economical hydrothermal method. The photocatalytic activity of Zn doped WO_3 nanoplates was studied by degradation of Congo red dye under visible light radiation. The effects of different experimental parameters like the dye concentration, photocatalyst dose and pH on the photocatalytic efficiency were explored under identical conditions. The kinetics study shows that the photocatalytic degradation follows first order kinetics. The photocatalytic degradation was found to enhance with increased Zn-doped WO_3 nanoplates. If the effect of Zn doping compared, then photocatalytic degradation efficiency for 5 wt.% Zn doped WO_3 was highest. The inclusion of Zn in the lattice of WO_3 was observed to be distinctive enough to enhance their photo-degradation efficiency under visible-light. Further, Zn doping not only restricts the recombination of photo induced electron–hole pairs but also enhances the photostability of WO_3.

Keywords: Congo red, Tungsten trioxide, Photocatalysis, Kinetics, Thermodynamic study.

INTRODUCTION

The conventional biological treatment methods are insufficient to degrade organic pollutants truly from wastewater [1,2]. Nanotechnology was tested to be effective process for wastewater treatment. The fast-moving developments in the field of nanotechnology have stimulated considerable research efforts on the synthesis and manufacturing of novel devices for various high-technological potential applications [3]. Recently, heterogeneous photocatalysis has gained an enormous attraction as it facilitates a simple, cheaper and effective way for the degradation of various organic pollutants [4]. Tungsten trioxide (WO_3) is one of the most interesting semiconductors in the fields of material science and metallurgy used for various industrial applications. Nanocrystalline WO_3 has initiated its value for breaking most refractory organic pollutants including dyes, detergents, pesticides and herbicides under UV-light irradiation [5], photocatalytic splitting of water to hydrogen and oxygen [6]. Another advantage of WO_3 is its outstanding photostability in acidic medium, which makes it a efficient photocatalyst for treating wastewater contaminated by organics [7]. However, the photocatalytic performance of WO_3 has limitations; comparatively wide band gap (2.8-3 eV) allows the excitation of electrons through near ultraviolet (UV) regions of the solar spectrum, which confines charge separation ability. The photocatalytic efficacy of WO_3 can be improved by narrowing the band gap of the photocatalyst [7-11]. For industrial applications, it is expected that the catalyst should have photocatalytic efficiency in visible or solar light. Doping of transition metal ions could extend photocatalytic applicability of WO_3 in visible/solar light. Further, transition metal ion dopants may restrict the recombination rate of photoinduced electron/hole pairs, which can significantly contribute for better photocatalytic efficiency [12,13].

The concentration of dopant could play a vital role in photocatalytic degradation, as the amount of dopant impacts the phenomenon of charge carrier trapping, separation and recom-

bination rate of photoinduced electron hole pair [14,15]. Very low dopant content does not affect the phenomenon of charge carrier generation, whereas high content of metal ion doping results in the formation of extra recombination sites, which could shorten the lifespan of photogenerated electrons and holes. Therefore, it is necessary to optimize dopant concentration for enhancing photocatalytic degradation process [16]. The optimum concentration of dopant depends on numerous factors, like the type of dopant selected, the coating deposition technique, annealing conditions, *etc.* [17].

In present work, the synthesis and characterization of WO_3 and Zn doped WO_3 layered nanosheets are reported by simple and economical hydrothermal method. The enhancement of visible light induced photocatalytic activity of Zn doped WO_3 layered nanosheets was examined for degradation of Congo red dye. The effect of several parameters such as contact time, pH of dye solution, catalyst dose on photocatalysis under visible light accompanied by the degradation kinetics for Congo red (CR) dye with as-prepared catalyst were also studied.

EXPERIMENTAL

All the reagents were of analytical grade (A.R.) and used without further purification. Sodium tungustanate ($Na_2WO_4 \cdot 2H_2O$) and Congo red dye were procured from Loba Chemie Pvt. Ltd., India, whereas citric acid and zinc chloride was procured from Merck Ltd, India. The concentration of the Congo red dye was determined by measuring absorbance using UV-VIS double beam spectrophotometer (Systronics model-2203) at the λ_{max} 495 nm. The pH was maintained using 0.1 M HCl and 0.1 M NaOH with pH meter (EQ-615).

Solution of different concentrations were prepared from the stock solution of Congo red dye in distilled water and pH maintained to 5. The WO_3 and Zn doped WO_3 nano catalyst was added in 50 mL Congo red solution taken in the photoreactor. Then solution was stirred for 60 min in dark in order to ensure the attainment of adsorption equilibrium. The dye sensitized WO_3 and Zn doped WO_3 was exposed to the visible light irradiation for the photodegradation of Congo red dye. The solution was analyzed after the separation of catalyst for determination of concentration of Congo red dye at λ_{max} 495 nm. Then influence of different parameters like initial concentration of dye, catalyst dose and effect of pH on the Congo red dye degradation kinetics was studied.

Synthesis of WO_3 and Zn doped WO_3: The WO_3 was synthesized by hydrothermal method using $Na_2WO_4 \cdot 2H_2O$ as precursor. In brief, 1.0 g of $Na_2WO_4 \cdot 2H_2O$ was mixed with 0.3 g of citric acid in 60 mL distilled water with stirring for 30 min. Then, 8 mL of 3 M HCl was added into the aqueous solution. and again stirred the solution for 10 min. The resulting mixture was transferred into a Teflon-lined stainless-steel autoclave, sealed and treated at 120 ºC for 24 h [18]. For the synthesis of different composition Zn doped WO_3 nanoparticles, the calculated amount of $ZnCl_2$ was introduced in precursor mixture before starting reaction [19]. After the completion of hydrothermal reaction, the product was washed with distilled water for several times in order to ensure complete removal of the ions possibly remaining in the final product and finally dried in air at 60 ºC overnight. By annealing the as-synthesized powder at 550 ºC for 4 h, nanocrystalline WO_3 was obtained [20].

RESULTS AND DISCUSSION

FESEM analysis: The FESEM images of WO_3 and zinc doped WO_3 nanosheets are shown in Fig. 1a-d. The SEM image of WO_3 and Zn doped WO_3 nanocatalyst shows nanoplates with thickness of ~20-34 nm with well-ordered and uniform crystal structure having regular size have very low grade of aggregation. The average crystallite size of WO_3 was found to be 48 nm and it further reduced to 36 nm for 5 wt.% Zn doped WO_3. This result reveals that the grain growth is suppressed due to doping of Zn into W-site [21]. The particle size found to decreases with increasing doping concentration of zinc.

Electron dispersive X-ray spectroscopy (EDS) analysis: Fig. 2a-d shows the elemental analysis of WO_3, Zn doped WO_3 nano catalyst. WO_3 contains only W K 80.70 %, O K 19.30 %. The 1 % Zn doped WO_3 contains W K 67.90 %, O K 32.08 % and Zn 0.02 %, The 2 % Zn doped WO_3 contains W K 79.61 %, O K 20.61 % and Zn 0.07 %. And the 5 % Zn doped WO_3 contains W K 81.50 %, O K 18.29 % and Zn 0.21% in EDS of and Zn doped WO_3 micrograph indicates the existence of WO_3 and Zn doped WO_3 in the nanocatalysts.

XRD studies: The crystalline phases of undoped and doped WO_3 nanoplates were recorded by X-ray diffraction patterns and are shown in Fig. 3. The major peaks at $2\theta \approx 16.486^\circ$, 23.669°, 25.638°, 33.362°, 34.249°, 34.963°, 38.014°, 38.922°, 42.86°, 49.135°, 52.553°, 54.175°, 56.145°, 57.226°, 58.286°, 61.337°, 62.787°, 66.01°,72.111°, 74.04°, 78.927°, corresponding to lattice planes (0 2 0), (1 2 0), (1 1 1), (0 4 0), (2 0 0), (0 0 2), (2 2 0), (0 2 2), (1 2 1), (2 0 2), (2 2 2), (1 6 0), (3 1 1), (1 6 1), (2 5 1), (2 4 2), (1 3 3), (1 7 1), (4 0 0), (2 7 1) and (3 1 3) confirms the crystalline orthorhombic structure of prepared samples and match with JCPDS data (84-0886).

The lattice parameters of orthorhombic pure and doped WO_3 have been determined [18] by following eqn. 1:

$$\frac{1}{d^2} = \frac{h^2}{a^2} + \frac{k^2}{b^2} + \frac{l^2}{c^2} \quad (1)$$

While the volume of orthorhombic pure and doped WO_3 by following eqn. 2:

$$v = abc \quad (2)$$

where (a, b, c) are the lattice parameters; d is the inter-planar distance and (*h*, *k*, *l*) are the Miller indices of the plane.

The crystallite size (D) was calculated by using Debye Scherrer's formula:

$$D = \frac{K\lambda}{\beta \cos\theta} \quad (3)$$

where λ is the wavelength of the X-ray radiation (λ = 1.5416 Å); K is the shape factor (0.9); β is the FWHM in radians; θ is the Bragg's angle.

Various structural parameters of undoped and doped WO_3 calculated by XRD data is tabulated in Table-1.

Effect of pH: The impact of pH on photocatalytic degradation of Congo red dye was investigated and the results obtained are shown in Fig. 4. The natural pH of 20 mg/L Congo red dye

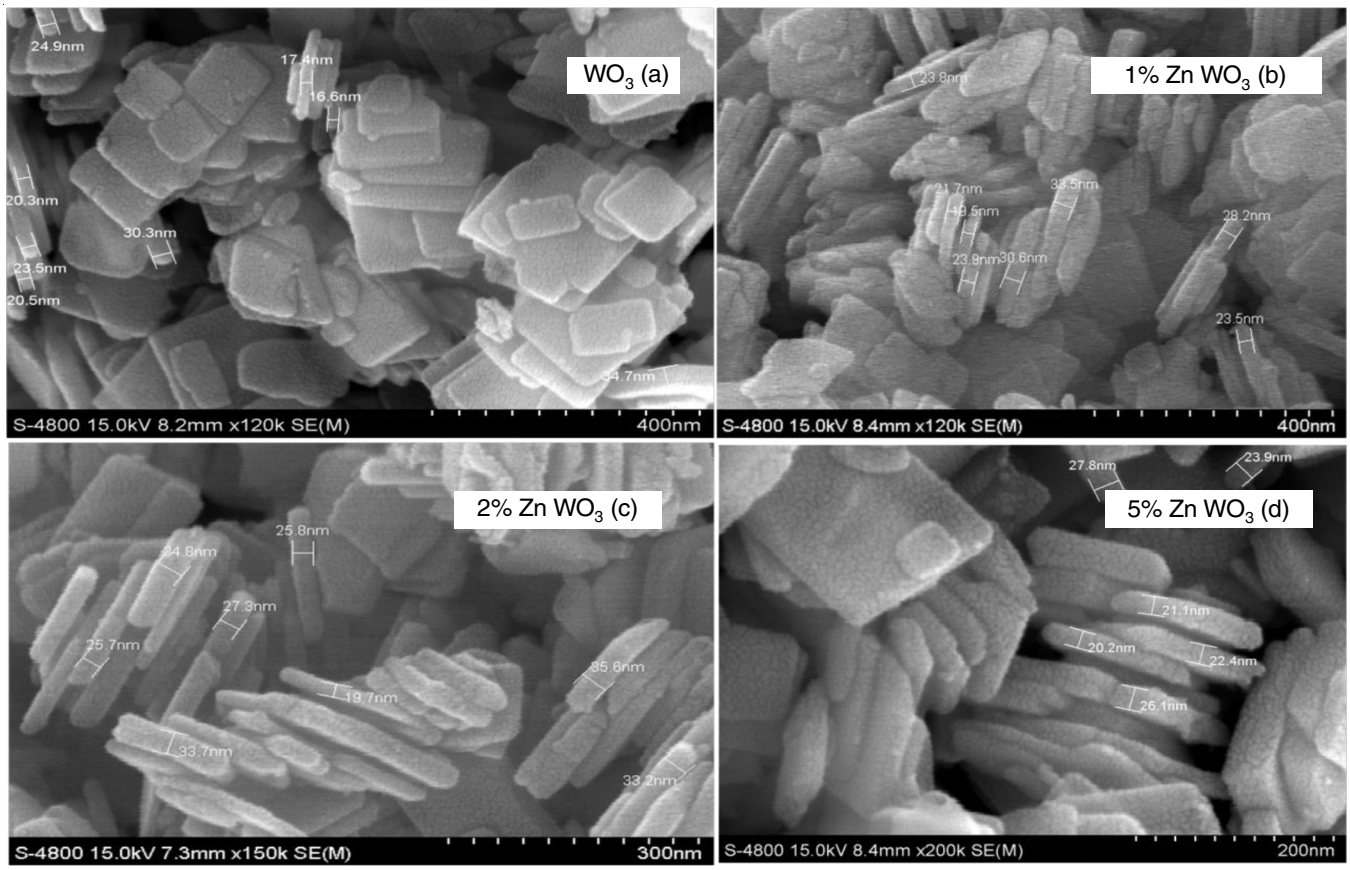

Fig. 1. SEM images of WO_3 and Zn doped WO_3 nanoplates

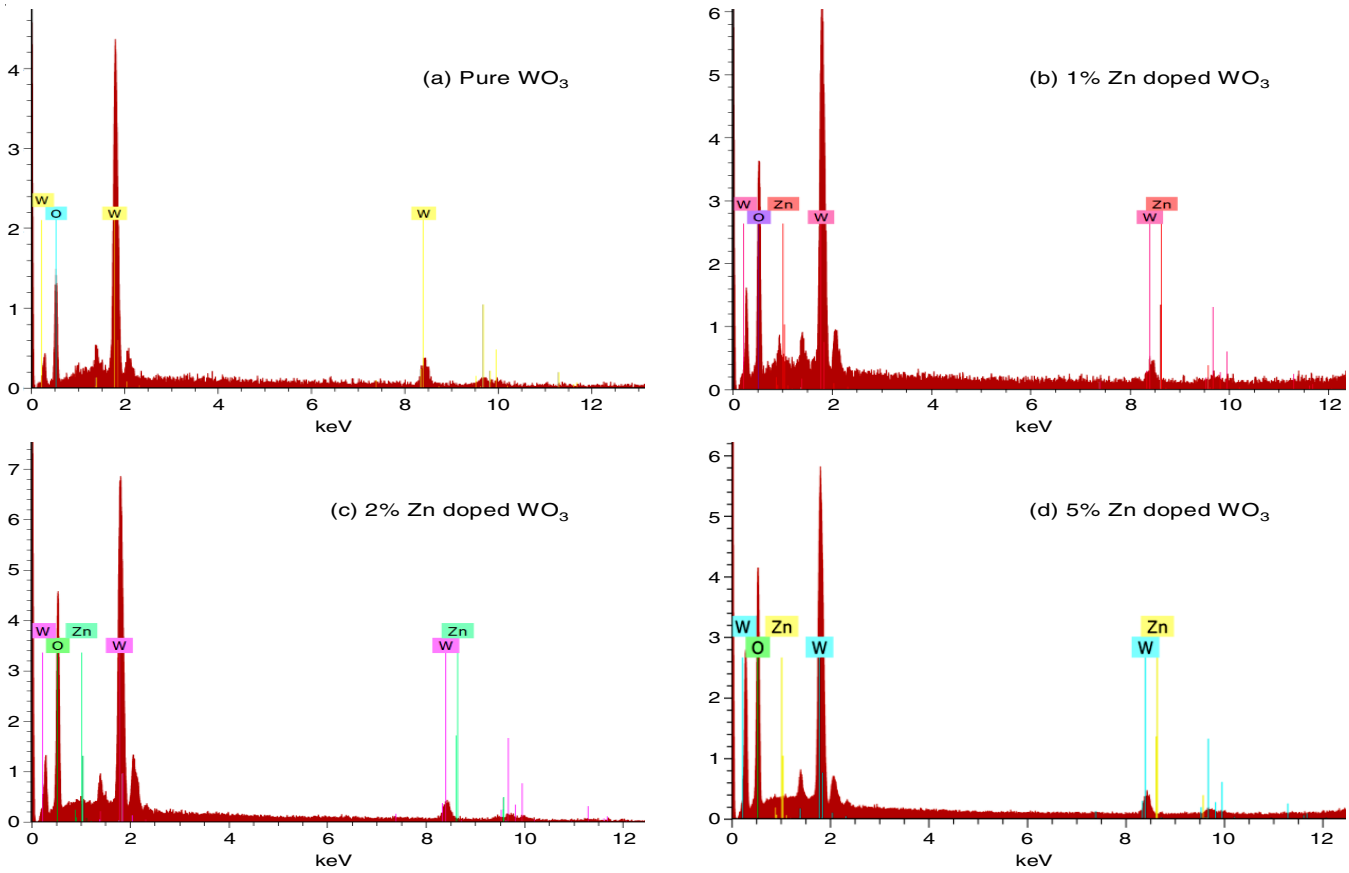

Fig. 2. The EDX spectrum of WO_3 and Zn doped WO_3 nanoplates

TABLE-1
STRUCTURAL PARAMETERS OF PURE AND DOPED WO_3 NANOPLATES

Samples	Lattice parameters			Volume (Å)	X-ray	Crystallite size (mm)
	a	b	c			
WO_3	5.1850	10.5222	5.1756	282.368	5.8796	40.1183860
1% Zn doped WO_3	5.1734	10.6899	5.1564	285.165	5.8219	37.2875230
2% Zn doped WO_3	5.2953	10.5706	5.0417	282.207	5.8829	41.6404540
5% Zn doped WO_3	5.1640	10.6554	5.1602	283.937	5.8471	41.6650982

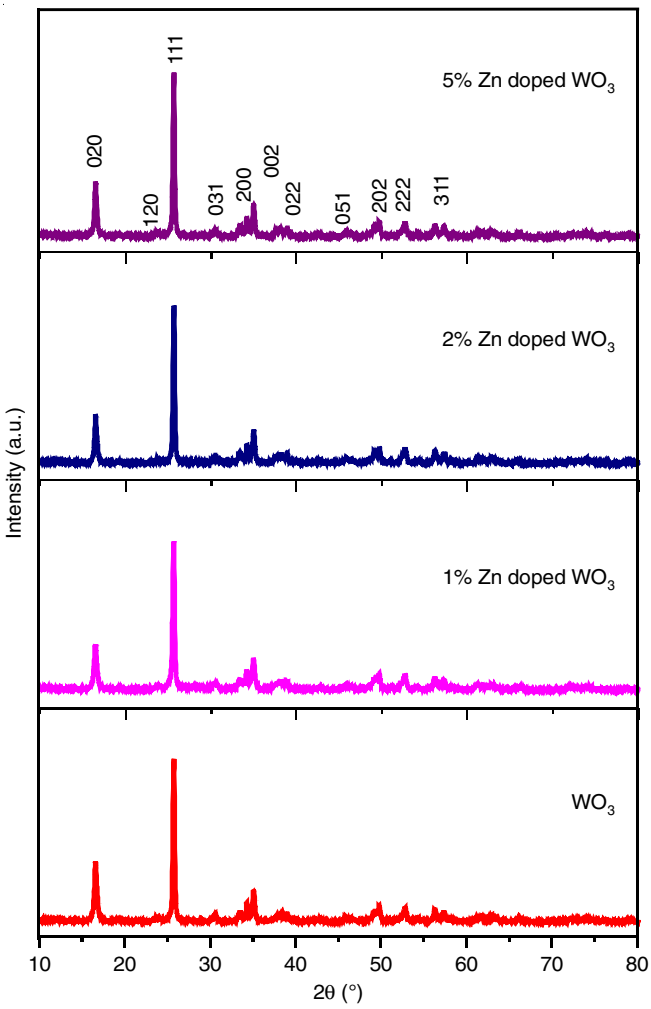

Fig. 3. XRD patterns of pure and Zn doped WO_3 nanoplates

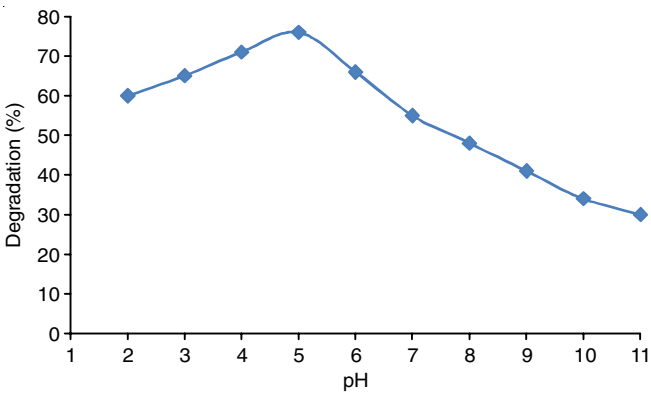

Fig. 4. Effect of pH on photocatalytic degradation of Congo red dye (conc. 20 mg/L, catalyst dose 1.0 g/L and time 120 min)

is 5. The percentage degradation of Congo red dye is lower in alkaline media that increases with decrease in pH, up to 5, the % degradation decreases and higher degradation is observed to acidic medium. The pH 5 is suitable for degradation of Congo red in presence of Zn doped WO_3 nanocatalyst for photocatalytic degradation. The WO_3 surface is positively charged in acidic medium and above this pH, the surface is negatively charged due to adsorbed OH^- ions. The Congo red being an anionic dye, attracted towards the nanocatalyst surface in the acidic medium. Various studies reveals that the photocatalytic removal of azo dyes like Congo red, proceeds through the breakdown of chromophore azo group generating N_2 [22].

$$R–N = N–R' + 2^{\bullet}OH \longrightarrow N_2\,(g) + ROH + R'OH \quad (4)$$

Congo red dye was oxidized by oxidative species like $^{\bullet}OH$ and converted into fatty acids through hydroxylation of aromatic rings by $^{\bullet}OH$, ring openings and photo–Kolbe decarboxylation reactions and finally into CO_2 until total mineralization [22,23].

Effect of doping on dye degradation: The influence of catalyst doping on initial dye concentration of Congo red was performed by varying the doping amount Zn in WO_3 as 1%, 2% and 5% using 1 g/L of nanocatalyst at pH 5. The results indicates that dye concentration reduces from 20 mg/L to 2.01 mg/L for WO_3, 20 mg/L to 1.22 mg/L for 1% Zn doped WO_3, 20 mg/L to 1.02 mg/L for 2% Zn doped WO_3 and 20 mg/L to 0.88 mg/L for 5% Zn doped WO_3 (Fig. 5). The reason is as doping concentration enhances, the unadsorbed dye concentration in the solution reduces. It causes more penetration of light through the solution on to the surface of WO_3 and Zn doped WO_3 consequently enhance the concentration of $^{\bullet}OH$ radicals on the surface and thus improves the percentage degradation [24].

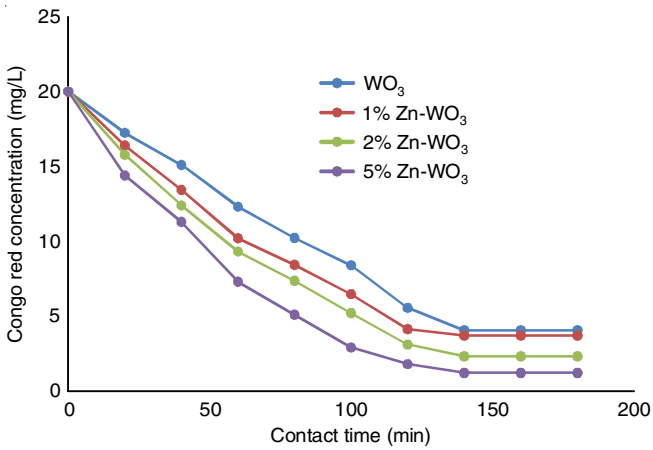

Fig. 5. Effect of catalyst on initial dye concentration (Congo red conc. 20 mg/L, pH 5, catalyst dose = 1.0 g/L)

Fig. 6 shows the effect of various doping ratios on the photocatalysis of Congo red dye. The optimized catalyst dose was 1 g/L, Congo red concentration was 20 mg/L and pH was 5. As shown in Fig. 6, the Congo red degradation was increased with the increase of Zn doping from 1 to 5%. The photocatalytic efficiency improves with improvement in doping concentration. The band gap energy decreases upon increase in doping from WO_3 to 5% Zn doped WO_3 [20,21]. Doping involves a facile substitution of W ions by Zn ions due to the similar ionic radius of Zn^{2+} and W^{6+}, which may create more oxygen vacancies for charge compensation. Again, fast transfer of the electrons from the WO_3 to the Zn may enhance the photocatalytic activity and increase the efficiency of photocatalytic degradation. This results in improvement of the photocatalytic efficiency of WO_3 [21].

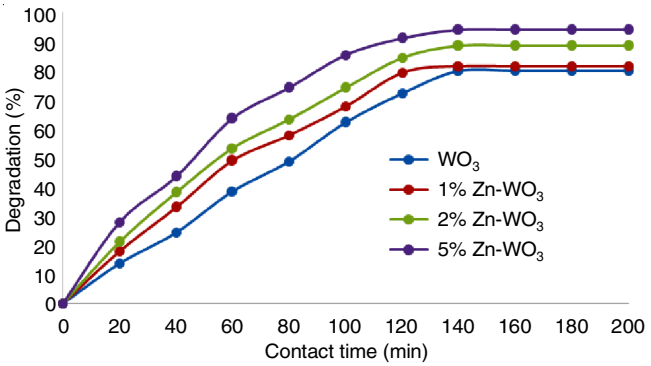

Fig. 6. Effect of doping percentage on percentage degradation of Congo red dye (catalyst dose 1 g/L, pH = 5 Congo red conc. = 40 mg/L and reaction time 120 min)

Effect of catalyst loading: To avoid the use of excess of catalyst, the optimum catalyst dose was determined using various concentrations of WO_3. It was found that initially the rate of degradation improves with the increase in catalyst dose, but afterwards it remains almost constant. Fig. 7 indicates that after 1 g/L of catalyst dose, % degradation remains almost constant. Therefore, 1 g/L was found to be the optimum catalyst dose [17]. The increase in catalyst dose has a positive impact on the number of photons absorbed and number of dye molecules adsorbed, thus, the dye degradation rate improves. After a certain catalyst dose, the number of dye molecules are inadequate to fill the surface active sites of WO_3. Thus, further increase in catalyst dose does not increase the degradation rate. This may be due to the decrease in the light penetration with an additional amount of WO_3. It also makes the solution more turbid and light penetration is impeded from the sample [18,19].

Effect of doping percentage and initial dye concentration: The degradation of Congo red dye at various concentrations (10, 20, 30 and 40 mg/L) for a catalyst dose of 1 g/L of 5 % Zn doped WO_3 nanocatalyst was studied and shown in Fig. 8. The degradation efficacy was to be inversely proportional to the increase in concentration. As the dye concentration increases, the equilibrium adsorption of the dye on the surface-active sites of the photocatalyst increases, therefore resulting in the lowering in rate of formation $^{\bullet}OH$ radicals, which is the principal oxidant in this process [22]. Again, the catalyst has a fixed number of

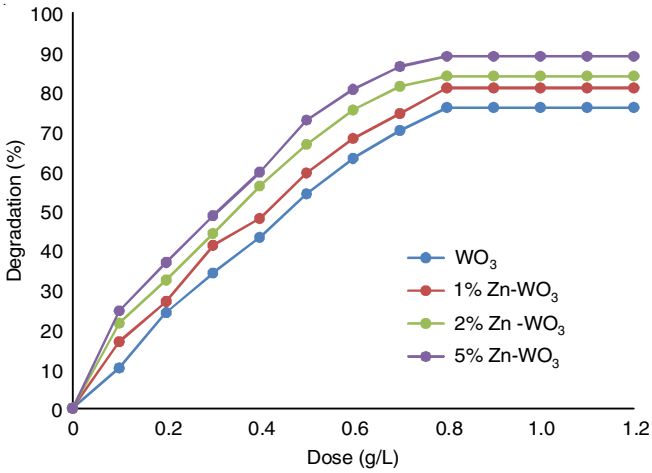

Fig. 7. Effect of dose on percentage degradation of Congo red dye (pH = 5, Congo red conc. = 40 mg/L and reaction time 120 min)

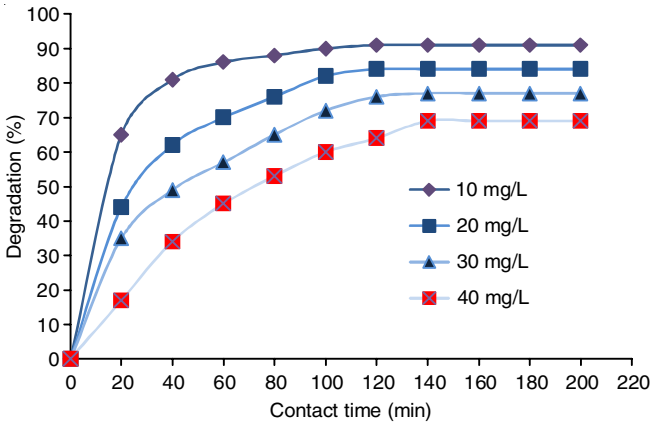

Fig. 8. Effect of initial dye concentration on photocatalytic degradation Congo red dye (pH 5, catalyst dose 1 g/L)

active sites available for adsorption for optimized dose. Therefore, when dye concentration is lower, dye gets easily absorbed while when dye concentration is higher, dye species have to compete on a limited number of active surface sites. This results in lowering of adsorption and photodegradation with increase in dye concentration. The maximum degradation 91% was observed for 10 mg/L Congo red dye concentration; it decreased down to 69% for 40 mg/L Congo red dye concentration. It indicates that an increase in concentration of dye causes a decrease in the percentage degradation.

Degradation kinetics: The photocatalytic degradation of Congo red dye by WO_3 nanocatalyst follows pseudo-first-order kinetics:

$$-\frac{dc}{dt} = k_{app}c \quad (4)$$

Integration of the above equation gives the following relation:

$$\ln\left(\frac{C_o}{C}\right) = k_{app}t \quad (5)$$

where C and C_o are the dye concentration at time t = t and t = 0, respectively and k_{app} is apparent reaction rate constant and t is time. According to the equation, a plot of $\ln(C_o/C)$ *versus* t

will give a slope of k_{app}. The linearity of the plot (Fig. 9) suggests that the photocatalytic degradation reaction follows pseudo-first-order kinetics with k_{app} of 0.00742 min^{-1}, 0.00992 min^{-1}, 0.01184 min^{-1} and 0.01438 min^{-1} for WO_3, 1% Zn doped WO_3 photocatalyst, 2% Zn doped WO_3 photocatalyst and 5% Zn doped WO_3 photocatalyst, respectively.

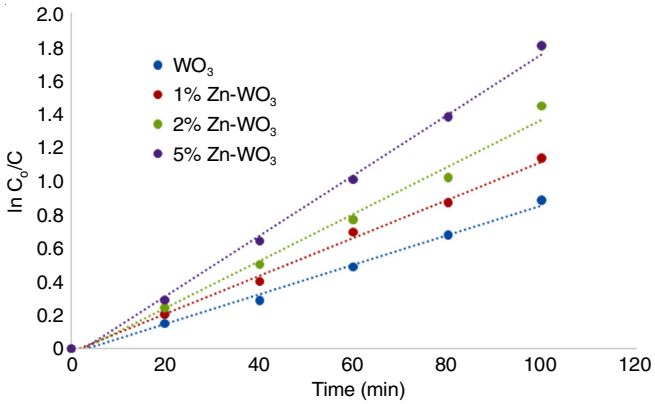

Fig. 9. First order kinetics plot of Congo red dye degradation with doped and undoped WO_3 photocatalyst (Congo red conc. = 20 mg/L, catalyst dose = 1 g/L, pH = 5 and reaction time 120 min)

Thermodynamic study of photocatalytic degradation of Congo red dye: The effect of temperature on photocatalytic degradation of Congo red was studied in the temperature range 298.15-318.15 K by using more effective 5% Zn doped WO_3 keeping other experimental parameters constant at dye concentration of 20 mg/L, 5% Zn doped WO_3 catalyst dosage was 0.5 g/L, pH dye solution equal to 5. The results are listed in Tables 2 and 3 and plotted in Figs. 10 and 11. It was observed that increase in temperature slightly increases % degradation and also the rate of reaction. This phenomenon might be explained in term of •OH generation as a function of temperature [25,26]. These results indicate that the degradation efficiency only slightly affected with the increase of temperature, according to Arrhenius law the rate of most reactions varies with temperature in the following manner:

$$K = Ae - \frac{E_a}{RT} \quad (6)$$

The activation energy (E_a) was calculated from the Arrhenius plot of ln k *vs*. 1/T, the slope of linear plot is equal to $-E_a/R$ as shown in Fig. 10. The entropy of activation (ΔS) was calculated from eqn. 7:

$$\ln A = \ln K_B \frac{T}{h} + \frac{\Delta S}{R} \quad (7)$$

TABLE-2
RATE CONSTANT VALUES FOR PHOTOCATALYTIC DEGRADATION OF CONGO RED DYES AT (298.15-318.15) K IN PRESENCE OF 0.5 g/L 5% Zn doped WO_3

Temp. (K)	K (min^{-1})	1/T	ln k
298.15	0.01642	0.003354	-4.1092
303.15	0.01932	0.003298	-3.9466
308.15	0.02259	0.003245	-3.7902
313.15	0.02630	0.003193	-3.6381
318.15	0.03047	0.003143	-3.4910

TABLE-3
KINETICS AND THERMODYNAMIC VALUES FOR THE PHOTOCATALYTIC DEGRADATION OF CONGO RED IN PRESENCE OF 5% Zn DOPED WO_3

Temp. (K)	K (min^{-1})	E_a (KJ mol^{-1})	ΔH (KJ mol^{-1})	ΔS (KJ mol^{-1} K^{-1})	ΔG (kJ mol^{-1})
298.15	0.01624	35.2537	26.34	-0.23	94.88
303.15	0.01932	35.2537	26.29	-0.23	94.83
308.15	0.02259	35.2537	26.24	-0.23	94.78
313.15	0.02630	35.2537	26.19	-0.23	94.73
318.15	0.03047	35.2537	26.17	-0.23	94.71

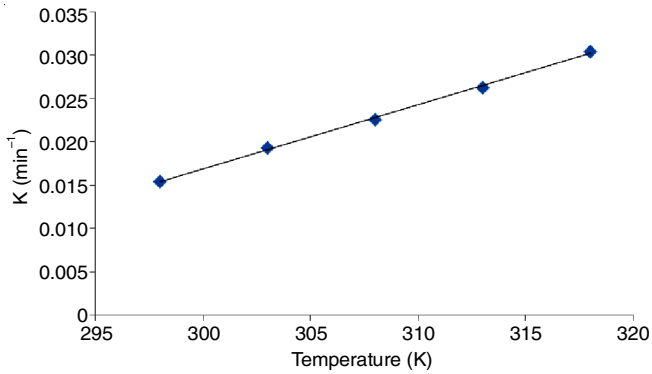

Fig. 10. Effect of temperature on photocatalytic degradation rate of Congo red dye in presence 0.5 g/L of 5% Zn doped WO_3

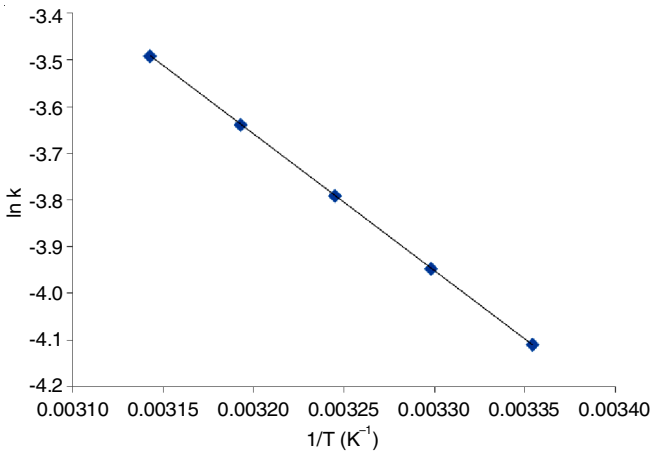

Fig. 11. Arrhenius plot of photocatalytic degradation of Congo red dye

where k = rate constant (first order, sec^{-1}), ln A = intercept with y variable, K_B = Boltzmann constant (1.38066×10^{-23} J K^{-1}); R = universal gas constant (8.31441 J mol^{-1} K^{-1}); h = Planck constant (6.6262×10^{-34} J s). The enthalpy of activation (ΔH) was calculated eqn. 8:

$$\Delta H = E_a - RT \quad (8)$$

The free energy of activation (ΔG) was calculated from eqn. 9:

$$\Delta G = \Delta H - T\Delta S \quad (9)$$

The results are listed in Table-3. The activation energy for photodegradation and decolorization of Congo red solutions by using 5% Zn doped WO_3 catalyst in the temperature range 298-318 K was equal to 35.2537 KJ mol^{-1}. The obtained lower activation energy is in good agreement with other literature as expected [27]. The role of catalyst is to proceed the reaction

by lowering the activation energy [28,29]. It is well known that irradiation is the primary source of electron–hole pair generation which is responsible for initiation of photoreaction, so the photocatalytic systems do not require heating and operate at near ambient temperature [30,31]. The true activation energy for photocatalytic systems E_a is nil, whereas the apparent activation energy E_a is often very low (a few kJ/mol) in the medium temperature range (20-80 ºC) [32]. The activation energy of photo catalysis reaction is reported as 5 to 35 kJ/mol in the literature [28]. However, at very low temperatures (-40 to 0 ºC) adsorption of final products formed favours, desorption of which tends to be the rate-limiting step. Due to its slower rate compared to the deterioration on the surface and the adsorption of reactants onto the catalyst's surface. At high temperatures (>70-80 ºC) for different types of photocatalytic reactions, the limited stage is the adsorption of dye on the surface of catalyst [26,33]. The positive ΔH denotes to endothermic reaction, the positive ΔG obtained indicates that the reaction is non-spontaneous. Positive ΔG could be because the activated state is a well solvated structure formed between the dye molecules and the reaction intermediates that is hydroxyl radicals which is also supported by negative entropy of activation. In present case, the value of ΔS is negative as in Table-3, so that the complex formed is more ordered than the reactants. Initially the complex formed is unstable and degradation of the reactants into products takes place rapidly under present set of experimental conditions [28].

Recycle performance of Zn doped WO_3 nanocatalyst: To find out the cost effectiveness of the process, stability and efficiency of Zn doped WO_3 nanocatalyst, Zn doped WO_3 nanocatalyst was reused for the % degradation of Congo red. For recycle study, the powdered nanocatalyst was centrifuged at the end of each photocatalytic run. The recovered sample was recycled for 3 times under similar experimental conditions. Fig. 12 shows that % degradation of Congo red dye by Zn doped WO_3 nano catalyst after 1st run was 96.5% (100 min). After the 4th run, it decreased down to 92.38%. The photocatalytic activity slightly decreases after the 4th run. This decrease may be due to loss of reused catalyst during sampling every time and irreversible changes of the surface of the photocatalyst by pollutants. Hence, it was observed that Zn doped WO_3 exhibit outstanding stability and does not suffer from corrosion during photocatalysis.

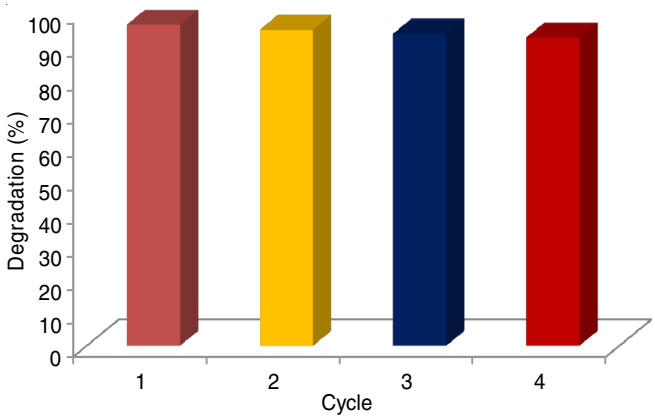

Fig. 12. Recycle study of Zn doped WO_3 nanocatalyst

Efficiency study of catalyst by effluent treatment: Total organic carbon (TOC) analysis of the sample is the most appropriate method for estimating the extent up to which the organic moieties in the effluent are degraded after treatment. TOC is the measure of the level of organic molecules or contaminants present in water [34,35]. The analysis of TOC offers a direct quantitative estimation of organic contamination in wastewater and natural water. To estimate the degradation level of organic contaminants TOC analysis of the sample before and after degradation was conducted along with other parameters like electrical conductivity, colour by absorbance at λ_{max}, associated with water quality by using the most efficient catalyst among synthesized doped and undoped photocatalyst. For this purpose, 0.5 g/L of 5% Zn doped WO_3 was used as it was found most efficient among all compositions of doped and undoped materials. The experimental set up was the same as used for the dye degradation process. The result is summarized in Table-4. The degradation results are near about the pollutants discharged by each plant are limited by a Central Pollution Control Board, New Delhi, India [36].

TABLE-4
EFFICIENCY STUDY OF THE CATALYST

Sample parameters	Before treatment	After treatment
pH	7.9	7.6
Electrical conductivity	15.96×10^{-3} mhos	11.57×10^{-3} mhos
TOC	325.6 ppm	35.48 ppm
Absorbance at λ_{max}	0.96	0.1

Conclusion

Aiming to more efficient photocatalytic semiconductor catalyst undoped and Zn doped WO_3 with different concentrations were synthesized. The XRD analysis of the synthesized samples with various attempts of synthesis confirms formation of WO_3 nanocatalyst. The composition of synthesized catalyst was detected by EDS analysis. From SEM analysis the plate shaped morphology was determined. The photocatalytic degradation of Congo red dye using nano-WO_3 and Zn doped WO_3 showed promising results towards removal of Congo red dye. The photocatalytic degradation followed pseudo-first-order kinetics with respect to Congo red dye. The percentage degradation of dye increased with an increase in catalyst loading and decrease with increase in pH, initial concentration of dye. The pH 5 found to be suitable for photocatalytic degradation of Congo red. A comparative study shows that 5% Zn doped WO_3 photocatalyst is more effective than bare WO_3, 1% Zn doped WO_3, 2% Zn doped WO_3 for photocatalytic degradation of Congo red with maximum degradation efficiency of 96.50%. The most efficient composition of catalyst 5% Zn doped WO_3 was effectively used for treatment of effluent discharge from a dyeing industry. The results of this analysis exhibited that the fabricated catalyst is excellent for pre-discharge treatment of effluent from the dyeing industry. This reveals the potential use of the photocatalyst on the industrial scale.

ACKNOWLEDGEMENTS

The authors gratefully acknowledged Central Instrumentation Centre, University Institute of Chemical Technology,

Kavayitri Bahimabai Chaudhari North Maharashtra University, Jalgaon, India for SEM, EDX and Department of Physics, Shivaji University, Kolhapur, India for XRD analysis. The authors have gratefully acknowledged Dr. Shirish Sonawane (NIT, Warangal) for providing TOC analysis and for his valuable suggestions. The authors are also thankful to Principal, Kisan Arts, Commerce and Science College, Parola, India, for providing necessary laboratory facilities and The Principal, S.R.N.D. Arts, Commerce and Science College, Bhadgaon, Dist. Jalgaon for providing necessary help for the work.

CONFLICT OF INTEREST

The authors declare that there is no conflict of interests regarding the publication of this article.

REFERENCES

1. C. Grandclément, I. Seyssiecq, A. Piram, P. Wong-Wah-Chung, G. Vanot, N. Tiliacos, N. Roche and P. Doumenq, *Water Res.*, **111**, 297 (2017); https://doi.org/10.1016/j.watres.2017.01.005
2. S.D. Melvin and F.D.L. Leusch, *Environ. Int.*, **92-93**, 183 (2016); https://doi.org/10.1016/j.envint.2016.03.031
3. M.H. Sayed Abhudhahir and J. Kandasamy, *J. Mater. Sci. Mater. Electron.*, **26**, 8307 (2015); https://doi.org/10.1007/s10854-015-3496-z
4. S. Rajendran, D. Manoj, J.N. Jebaranjitham, B.G. Kumar, G. Bharath, F. Banat, J. Qin, S. Vadivel and F. Gracia, *J. Mol. Liq.*, **311**, 113328 (2020); https://doi.org/10.1016/j.molliq.2020.113328
5. F. Mehmood, J. Iqbal, T. Jan and Q. Mansoor, *J. Alloys Compd.*, **728**, 1329 (2017); https://doi.org/10.1016/j.jallcom.2017.08.234
6. S. Adhikari, D. Sarkar and H.S. Maiti, *Mater. Res. Bull.*, **49**, 325 (2014); https://doi.org/10.1016/j.materresbull.2013.08.028
7. H. Zhang, G. Chen and D.W. Bahnemann, *J. Mater. Chem.*, **19**, 5089 (2009); https://doi.org/10.1039/b821991e
8. R.H. Coridan, M. Shaner, C. Wiggenhorn, B.S. Brunschwig and N.S. Lewis, *J. Phys. Chem. C*, **117**, 6949 (2013); https://doi.org/10.1021/jp311947x
9. M. Ahmadi, R. Younesi and M.J.-F. Guinel, *J. Mater. Res.*, **29**, 1424 (2014); https://doi.org/10.1557/jmr.2014.155
10. M.R. Waller, T.K. Townsend, J. Zhao, E.M. Sabio, R.L. Chamousis, N.D. Browning and F.E. Osterloh, *Chem. Mater.*, **24**, 698 (2012); https://doi.org/10.1021/cm203293j
11. X.F. Cheng, W.H. Leng, D.P. Liu, J.Q. Zhang and C.N. Cao, *Chemosphere*, **68**, 1976 (2007); https://doi.org/10.1016/j.chemosphere.2007.02.010
12. V. Hariharan, V. Aroulmoji, K. Prabakaran, M. Parthibavarman, B. Gnanavel, R. Sathyapriya and M. Kanagaraj, *J. Alloys Compd.*, **689**, 41 (2016); https://doi.org/10.1016/j.jallcom.2016.07.136
13. C.Y. Park, J.M. Seo, H. Jo, J. Park, K.M. Ok and T.J. Park, *Sci. Rep.*, **7**, 40928 (2017); https://doi.org/10.1038/srep40928
14. D. Sánchez-Martínez, A. Martínez-de la Cruz and E. López-Cuéllar, *Mater. Res. Bull.*, **48**, 691 (2013); https://doi.org/10.1016/j.materresbull.2012.11.024
15. N. Asim, M.F. Syuhami, M. Badiei and M.A. Yarmo, *APCBEE Procedia*, **9**, 175 (2014); https://doi.org/10.1016/j.apcbee.2014.01.031
16. S.P. Patil, V.K. Mahajan, V.S. Shrivastava and G.H. Sonawane, *Iran. Chem. Commun.*, **5**, 417 (2017).
17. M. Abdennouri, A. Elhalil, M. Farnane, H. Tounsadi, F.Z. Mahjoubi, R. Elmoubarki, M. Sadiq, L. Khamar, A. Galadi, M. Baalala, M. Bensitel, Y. El hafiane, A. Smith and N. Barka, *J. Saudi Chem. Soc.*, **19**, 485 (2015); https://doi.org/10.1016/j.jscs.2015.06.007
18. S. Bai, K. Zhang, X. Shu, S. Chen, R. Luo, D. Li and A. Chen, *CrystEngComm*, **16**, 10210 (2014); https://doi.org/10.1039/C4CE01167H
19. Y. Wang, B. Liu, S. Xiao, X. Wang, L. Sun, H. Li, W. Xie, Q. Li, Q. Zhang and T. Wang, *ACS Appl. Mater. Interfaces*, **8**, 9674 (2016); https://doi.org/10.1021/acsami.5b12857
20. B. Deepa and V. Rajendran, *Nano-Struct. Nano-Objects*, **16**, 185 (2018); https://doi.org/10.1016/j.nanoso.2018.06.005
21. D. Madhan, M. Parthibavarman, P. Rajkumar and M. Sangeetha, *J. Mater. Sci. Mater. Electron.*, **26**, 6823 (2015); https://doi.org/10.1007/s10854-015-3296-5
22. M. Alaei, A.R. Mahjoub and A. Rashidi, *Iran. J. Chem. Chem. Eng.*, **31**, 23 (2012); https://doi.org/10.30492/ijcce.2012.6042
23. A. Akyol, H.C. Yatmaz and M. Bayramoglu, *Appl. Catal. B*, **54**, 19 (2004); https://doi.org/10.1016/j.apcatb.2004.05.021
24. Q. Xiang, G.F. Meng, H.B. Zhao, Y. Zhang, H. Li, W.J. Ma and J.Q. Xu, *J. Phys. Chem. C*, **114**, 2049 (2010); https://doi.org/10.1021/jp909742d
25. M.T. Eesa, A.M. Juda and L.M. Ahmed, *Int. J. Sci. Res.*, **5**, 1495 (2016); https://doi.org/10.21275/ART20163016
26. K.M. Reza, A.S.W. Kurny and F. Gulshan, *Appl. Water Sci.*, **7**, 1569 (2017); https://doi.org/10.1007/s13201-015-0367-y
27. C. Ferrari, H. Chen, R. Lavezza, C. Santinelli, I. Longo and E. Bramanti, *Int. J. Photoenergy*, **2013**, 854857 (2013); https://doi.org/10.1155/2013/854857
28. K. Byrappa, A.K. Subramani, S. Ananda, K.M.L. Rai, R. Dinesh and M. Yoshimura, *Bull. Mater. Sci.*, **29**, 433 (2006); https://doi.org/10.1007/BF02914073
29. N. Barka, S. Qourzal, A. Assabbane, A. Nounah and Y. Ait-Ichou, *J. Photochem. Photobiol. Chem.*, **195**, 346 (2008); https://doi.org/10.1016/j.jphotochem.2007.10.022
30. Z.H. Siahpoosh and M. Soleimani, *Process Saf. Environ. Prot.*, **111**, 180 (2017); https://doi.org/10.1016/j.psep.2017.07.009
31. Z.M. Abou-Gamra, *Adv. Chem. Eng. Sci.*, **4**, 285 (2014); https://doi.org/10.4236/aces.2014.43031
32. W. Xie, Y.Z. Li, W. Sun, J.C. Huang, H. Xie and X.J. Zhao, *J. Photochem. Photobiol. Chem.*, **216**, 149 (2010); https://doi.org/10.1016/j.jphotochem.2010.06.032
33. K. Mehrotra, G.S. Yablonsky and A.K. Ray, *Chemosphere*, **60**, 1427 (2005); https://doi.org/10.1016/j.chemosphere.2005.01.074
34. G.H. Sonawane, S.P. Patil and V.S. Shrivastava, *J. Inst. Eng. India Ser. E*, **98**, 55 (2017); https://doi.org/10.1007/s40034-016-0089-1
35. V.K. Mahajan and G.H. Sonawane, *Nanochem. Res.*, **1**, 258 (2016); https://doi.org/10.7508/ncr.2016.02.013
36. www.cpcbenvis.nic.in